A Low-Voltage Test Setup for the Characterization of High-Voltage Active EMI Filters

Jacopo Serra, Markeljan Fishta, Franco Fiori
MicroEMC Group, Politecnico di Torino, Italy
franco.fiori@polito.it

***Abstract*—Active EMI filters (AEFs) are an effective solution for mitigating conducted electromagnetic disturbances in high-voltage (HV) power electronic systems. After design and prototyping, experimental validation is a critical step to ensure that the AEF meets the target performance. However, for HV designs, the testing process is often complex, time-consuming, and constrained by safety requirements. This paper proposes a low-voltage (LV) measurement setup for the validation and testing of AEFs intended for HV applications. The proposed approach reproduces disturbance levels comparable to those encountered in HV operation, while allowing the use of standard laboratory equipment and simplified safety procedures. Experimental results demonstrate that the LV setup enables reliable evaluation of AEF performance, providing a low-risk pre-validation method prior to full-scale HV testing.**

***Index Terms*—Conducted electromagnetic emissions, EMI filter, active EMI filter, hybrid EMI filter, high-voltage power converters.**

I. INTRODUCTION

Active EMI filters (AEFs) for high-voltage (HV) DC applications are being employed more and more, thanks to the increasing use of wide bandgap (WBG) devices in power converters [1]. Such converters enable higher power density with respect to silicon-based designs [2], meaning that the EMI filters required to make them compliant with emission regulations [3] have become the bottleneck to overall volume minimization [4]. In this context, AEFs are used to decrease the volume of EMI filters, at the cost of increased design complexity [5]. Indeed, AEFs include amplifier-based circuits, improving the filter attenuation at low frequency and relaxing the requirement on the passive filter components, which dominate the overall system volume and weight. AEFs base their operation on the sensing of a voltage or current disturbance and the injection of a suitable cancellation voltage or current, resulting in four possible topologies [5]. However, the Voltage Sensing Current Cancellation (VSCC) topology has become the most used thanks to the absence of additional magnetic components, which are needed for current sensing and voltage cancellation [6], [7], [8], [9].

One of the steps after the design and prototyping of an AEF, is its experimental validation and testing. However, the presence of a HV source in the test setup makes the process long, complex, and costly, due to safety constraints, specialized equipment, and limited measurement flexibility. For these reasons, this work proposes an experimental setup for the validation and testing of the AEF, using a low-voltage (LV) source, while ensuring a disturbance level close to that experienced in the HV application. The proposed approach enables faster iteration, facilitating AEF development with reduced experimental complexity.

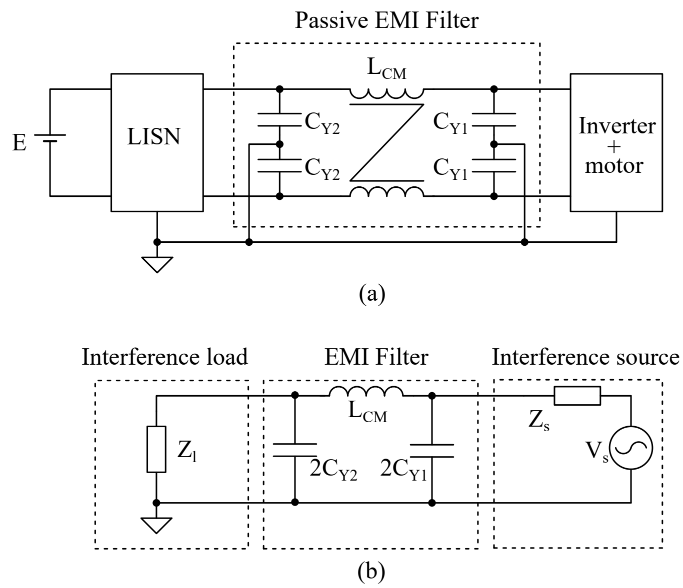

Fig. 1. Conducted EMI measurement bench of the system under consideration (a) and its CM equivalent circuit (b).

II. AEFS FOR HV APPLICATIONS

In this section, the interference source model and the AEF considered in this work are presented, providing the reference framework for the proposed validation approach.

A. *Interference source model*

The system under consideration is the one shown in Fig. 1(a). The unit under test is a DC-fed three phase inverter, loaded by an electric motor. A reference CLC Passive EMI Filter (PEF) is placed at the input, to make the inverter compliant with emission limits [3]. The inverter supply (E) is filtered by the line impedance stabilization networks (LISNs), which set the common mode and the differential mode impedance towards the DC supply. For the Common Mode (CM) emission estimation purpose, the CM equivalent circuit shown in Fig. 1(b) is employed. The interference load is given by the CM equivalent impedance of the LISNs (Z_{L}), while the interference source impedance is represented by (Z_{S}). Such an

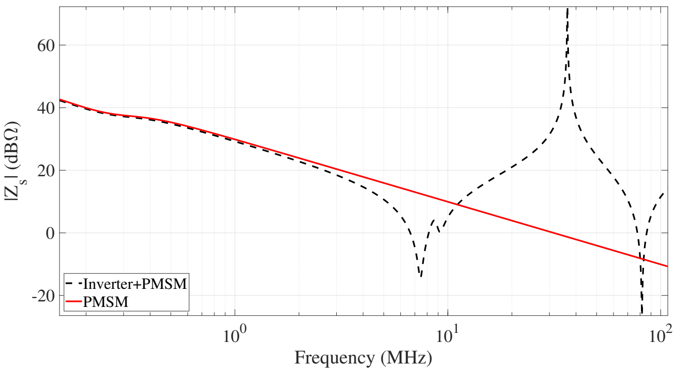

Fig. 2. Example of CM interference source impedance. The CM impedance of the motor only is shown by continuous line, that of the motor connected to the inverter through cables by the dashed line.

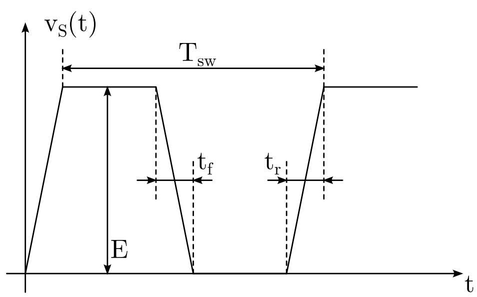

Fig. 3. CM interference source waveform.

impedance is determined by all the parasitic paths from the HV lines towards the chassis, the main ones being the parasitic capacitance of the switching devices towards the heatsink, the three-phase output cable, and the motor coupling to the chassis. An example of the behavior of such an impedance is given in Fig. 2. At Low Frequency (LF), up to a few MHz, the source impedance is capacitive and dominated by that of the motor, whereas at High Frequency (HF) the impedance is mainly determined by the cables and the stray parameters of the inverter. On the other hand, the interference voltage source $v_{\mathrm{S}}(t)$ represents the CM voltage at the output of the inverter. In the worst case scenario, i.e., the highest achievable CM emission level, the three output phases switch at the same time, meaning that the maximum CM current is injected into Z_{S}, which flows to the receiver. In such a case, the interference voltage can be approximated by a trapezoidal wave with amplitude E, frequency f_{SW} and transition times $t_{\mathrm{r}} = t_{\mathrm{f}}$, as shown in Fig. 3. The wave period is $T_{\mathrm{sw}} = \frac{1}{f_{\mathrm{sw}}}$ while the duty cycle is assumed fixed at $50\,\%$ for simplicity.

B. Hybrid EMI filter

AEF for HV power applications are usually included in Hybrid EMI filter like that shown in Fig. 4, because they provide a fictitious Y capacitance larger than the real one. This allows for reducing the overall size of the EMI filter [9]. The VSCC AEF considered in this work is that shown in Fig. 4 and it's CM equivalent circuit is in Fig. 5. About the circuit, the amplifier receives the HV line voltage at its input, and

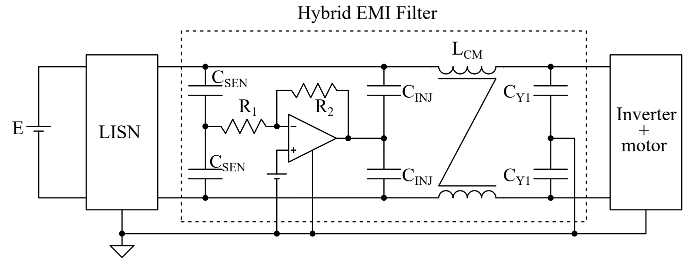

Fig. 4. Hybrid EMI filter inserted in the DC-link between the power inverter and the LISN.

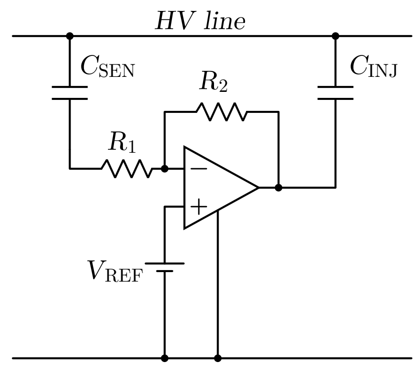

Fig. 5. CM equivalent circuit of VSCC AEF.

drives the injection capacitor with an amplified and inverted version of such a voltage, resulting in an injected cancellation current. A sensing capacitor (C_{SEN}) is introduced in the input branch, to keep the LV amplifier isolated from the HV lines. The equivalent impedance presented by the circuit between the HV line and reference ground (chassis), in band, is given by

$$Z_{\mathrm{eq}} \simeq \frac{1}{sC_{\mathrm{eq}}} \tag{1}$$

where

$$C_{\mathrm{eq}} = \left(1 + \frac{R_2}{R_1}\right) C_{\mathrm{INJ}} \tag{2}$$

resulting in an increased effective capacitance by a factor

$$G = 1 + \frac{R_2}{R_1}. \tag{3}$$

What follows shows the approach developed within the present work to validate and optimize the AEF in a low-voltage environment, which puts the AEF in operating conditions similar to the high-voltage ones.

III. Filter Characterization

Once an AEF has been designed and prototyped, laboratory testing is needed to validate the design and make sure that the target performance is met. The main performance metric of an EMI filter is its Insertion Loss (IL), which can be assessed under small-signal or under operating (large-signal) conditions. These two test setups and the difficulties related with the second, along with the proposed setup, are discussed in what follows.

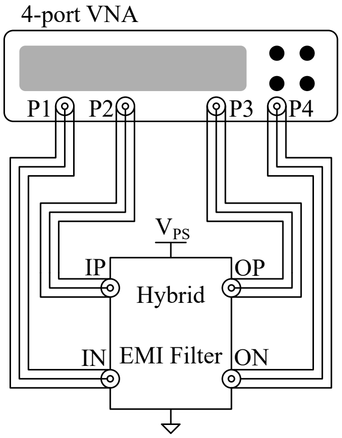

Fig. 6. 4-port S parameters measurement setup.

A. Small-signal characterization

Small-signal IL of the HEF is obtained from 4-port S parameter measurements. A schematic of the measurement setup is given in Fig. 6. The 4x4 scattering matrix of the filter is measured by means of a VNA. From these data, mixed-mode s-matrices

$$\mathbf{S}_{\mathrm{cc}} = \begin{bmatrix} s_{\mathrm{cc11}} & s_{\mathrm{cc12}} \\ s_{\mathrm{cc21}} & s_{\mathrm{cc22}} \end{bmatrix} \tag{4}$$

$$\mathbf{S}_{\mathrm{dd}} = \begin{bmatrix} s_{\mathrm{dd11}} & s_{\mathrm{dd12}} \\ s_{\mathrm{dd21}} & s_{\mathrm{dd22}} \end{bmatrix} \tag{5}$$

are evaluated [10]. The IL of the filter, for CM and DM, can be written as in (10) and (11), respectively, where

$$\rho_{\mathrm{scm}} = \frac{Z_{\mathrm{scm}} - Z_0/2}{Z_{\mathrm{scm}} + Z_0/2} \tag{6}$$

$$\rho_{\mathrm{lcm}} = \frac{Z_{\mathrm{lcm}} - Z_0/2}{Z_{\mathrm{lcm}} + Z_0/2} \tag{7}$$

$$\rho_{\mathrm{sdm}} = \frac{Z_{\mathrm{sdm}} - 2Z_0}{Z_{\mathrm{sdm}} + 2Z_0} \tag{8}$$

$$\rho_{\mathrm{ldm}} = \frac{Z_{\mathrm{ldm}} - 2Z_0}{Z_{\mathrm{ldm}} + 2Z_0} \tag{9}$$

with Z_0 being the port reference impedance, Z_{scm} being the CM source impedance, Z_{lcm} being the CM load impedance, Z_{sdm} being the DM source impedance, Z_{ldm} being the DM load impedance.

B. Operating conditions and proposed test setup

Besides small-signal IL measurements, tests should be also performed in the nominal operating conditions. In HV applications this means performing tests with the inverter being supplied with HV, making sure that the filter components experience the voltage swing as they would in the target application. Tests with HV equipment require complex procedures, due to safety reasons, leading to an increase of the required test time and cost. A solution to allow simple and quick debug and characterization of the AEF is presentd in what follows.

Since the AEFs are mainly effective at low frequency (up to a few MHz), the interference source impedance can be approximated as purely capacitive, C_{S}, resulting in the CM equivalent circuit of Fig. 7.

The interference source voltage v_{S}, the source capacitance C_{S} and the input filter capacitance C_{Y} form a voltage divider, as represented in Fig. 8, left. By using Thévenin's theorem, an equivalent model of the source can be derived, as in Fig. 8, right. The equivalent parameters are given by

$$C_{\mathrm{S,eq}} = C_{\mathrm{S}} + C_{\mathrm{Y}} \tag{12}$$

$$v_{\mathrm{S,eq}} = v_{\mathrm{S}} \frac{C_{\mathrm{S}}}{C_{\mathrm{S}} + C_{\mathrm{Y}}}. \tag{13}$$

The equivalent source voltage has the same shape as the HV one, with the scaled amplitude

$$E_{\mathrm{eq}} = E \frac{C_{\mathrm{S}}}{C_{\mathrm{S}} + C_{\mathrm{Y}}}. \tag{14}$$

Normally, for traction inverters, C_{S} is in the order of few nF and C_{Y} is in the order of a few hundred nF, meaning $C_{\mathrm{S}} \ll C_{\mathrm{Y}}$, so the required disturbance amplitude is effectively decreased, relaxing safety concerns related to HV testing. The resulting equivalent CM test setup is given in Fig. 9.

The required equivalent source capacitance can be easily obtained by selecting an appropriate capacitor, with value given by (12). To implement the interference source voltage, a low impedance trapezoidal wave generator is required. Traditional laboratory Arbitrary Wave Generators (AWGs) are not suitable for this task, as they normally have $50\,\Omega$ internal impedance, which causes the source waveform to be different from the required one. Moreover, such instruments usually have limited amplitude swing, of a few V, while depending on E, C_{S} and C_{Y}, E_{eq} can be up to a few tens of V. This paper proposes to implement the equivalent source voltage by means of a switching leg, like that shown in Fig. 10. The supply voltage of the switching leg should be set to match the required equivalent supply voltage E_{eq}, while its switching frequency should match that of the HV inverter under consideration (f_{sw}). Moreover, the transistor drive can be modulated to match the transition times of the reference waveform (t_{r}, t_{f}).

C. Simulation results

To validate the proposed approach, circuit simulations have been performed with the test setup of Fig. 7 and Fig. 9, respectively. The simulation parameters are given in Table I and Z_{L} is as specified by [3] for HV LISNs. The simulated waveforms for amplifier output voltage and output current are given in Fig. 11.

The results confirm that the proposed setup, with supply voltage $E_{\mathrm{eq}} = 4.78\,\mathrm{V}$ yields similar amplifier output voltage and current with respect to the HV setup, with supply voltage $E = 100\,\mathrm{V}$, meaning that the filter components are subject to similar solicitation in both cases.

$$IL_{\mathrm{cm}} = 20\log\left|\frac{(1-\rho_{\mathrm{scm}}s_{\mathrm{cc11}})(1-\rho_{\mathrm{lcm}}s_{\mathrm{cc22}})-\rho_{\mathrm{scm}}\rho_{\mathrm{lcm}}s_{\mathrm{cc12}}s_{\mathrm{cc21}}}{(1-\rho_{\mathrm{scm}}\rho_{\mathrm{lcm}})s_{\mathrm{cc21}}}\right| \quad (10)$$

$$IL_{\mathrm{dm}} = 20\log\left|\frac{(1-\rho_{\mathrm{sdm}}s_{\mathrm{dd11}})(1-\rho_{\mathrm{ldm}}s_{\mathrm{dd22}})-\rho_{\mathrm{sdm}}\rho_{\mathrm{ldm}}s_{\mathrm{dd12}}s_{\mathrm{dd21}}}{(1-\rho_{\mathrm{sdm}}\rho_{\mathrm{ldm}})s_{\mathrm{dd21}}}\right| \quad (11)$$

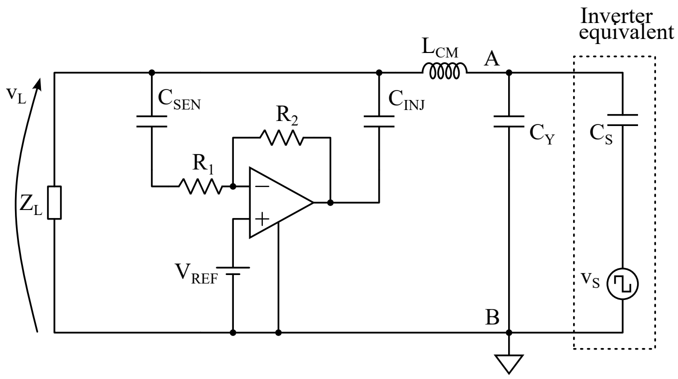

Fig. 7. CM equivalent circuit of the hybrid filter comprising an equivalent circuit of the source of switching noise (v_{S},Z_{S}) and the CM input impedance of the LISNs (Z_{L}).

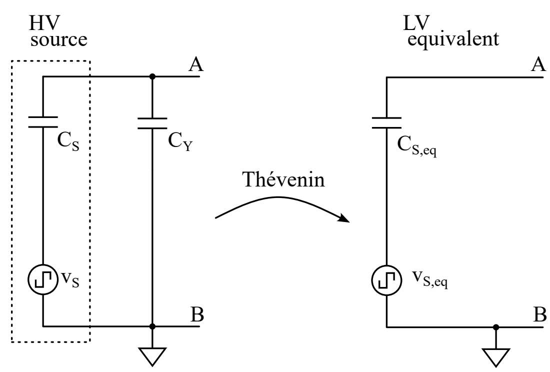

Fig. 8. CM equivalent circuit of the source of switching noise (left) and its Thévenin equivalent circuit (right).

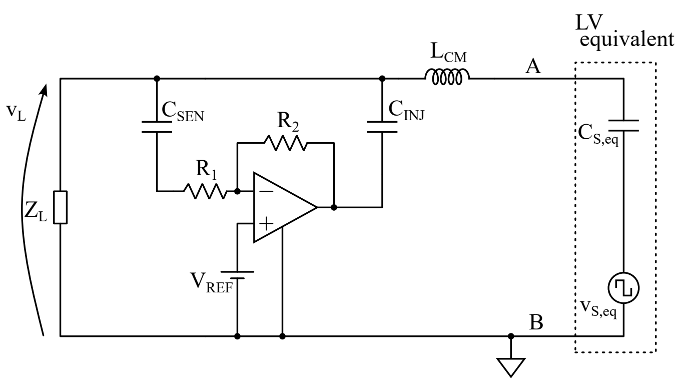

Fig. 9. CM equivalent circuit of the hybrid filter excited by the CM LV noise source ($v_{\mathrm{S,eq}}$, $Z_{\mathrm{S,eq}}$)

IV. Experimental results

The proposed technique was applied to the testing and validation of an AEF like that of Fig. 5. The AEF is tailored to a HV traction inverter system, with the specifications given in Table I. First of all, small-signal measurements were carried out and the resulting IL for a $50\,\Omega$ system is provided in Fig. 12. The IL measurements show that the AEF is only effective for CM attenuation, since the IL increases when the amplifier is turned on, while for DM the IL does not change when the amplifier is turned on. Next, the output voltage swing of the amplifier was measured, while operating at first with a three phase inverter loaded by a motor, supplied with HV source, and then while operating with a switching leg supplied with LV source. The system parameters were the ones provided in

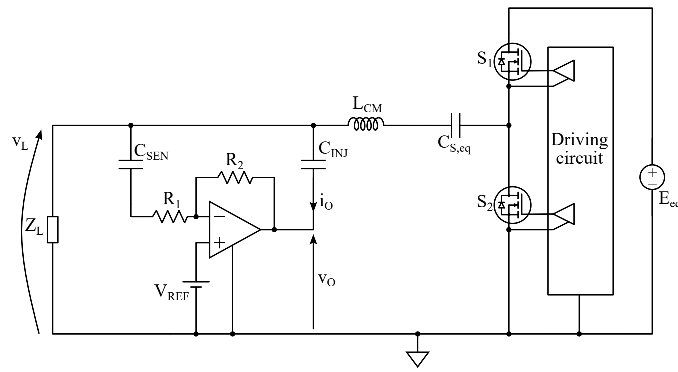

Fig. 10. Equivalent test setup.

TABLE I
System parameters.

Param.	Value	Unit	Param.	Value	Unit
E	100	V	f_{sw}	32	kHz
C_{S}	10	nF	t_{r}	100	ns
C_{Y}	200	nF	t_{f}	100	ns
C_{INJ}	200	nF	E_{eq}	4.78	V
C_{SEN}	2	nF	L_{CM}	100	µH
R_2	22	kΩ	R_1	2.4	kΩ

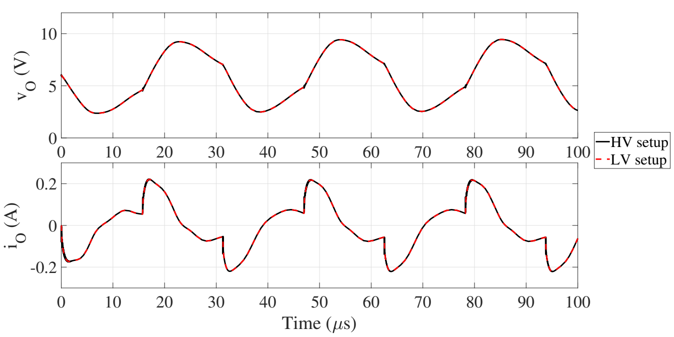

Fig. 11. Simulation results showing the AEF output voltage and current in the case of the HV and LV setup.

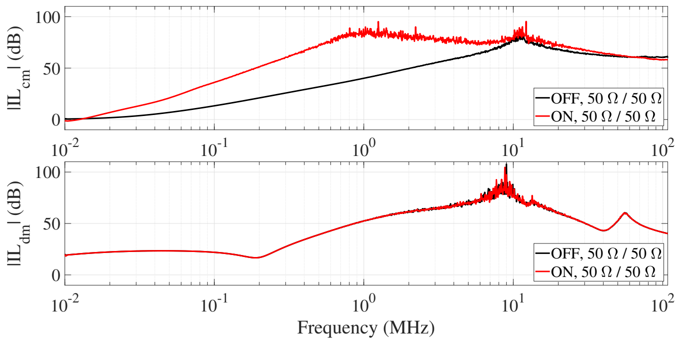

Fig. 12. Small-signal AEF IL experimental measurement results for CM and DM.

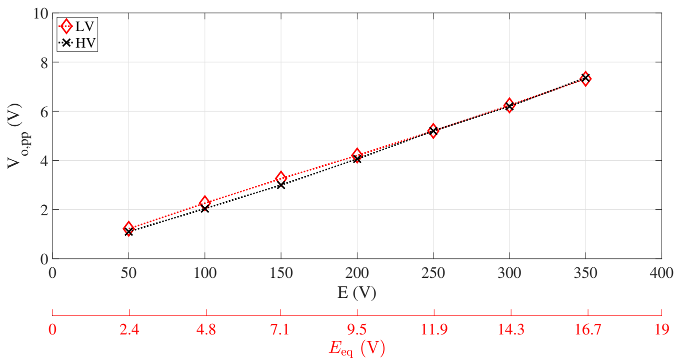

Fig. 13. Amplifier output swing experimental measurement results.

Table I, which result in

$$E_{\mathrm{eq}} = E\frac{C_{\mathrm{S}}}{C_{\mathrm{S}} + C_{\mathrm{Y}}} = \frac{E}{21} \tag{15}$$

and

$$C_{\mathrm{S,eq}} = C_{\mathrm{S}} + C_{\mathrm{Y}} = 210\,\mathrm{nF}. \tag{16}$$

All parameters were kept constant, while the inverter supply voltage, E, was varied. The amplifier output voltage swing measurement results are shown in Fig. 13. The resulting values for E between $50\,\mathrm{V}$ and $350\,\mathrm{V}$ are in good agreement for the case in which the AEF is under operating conditions with HV inverter and the case of the proposed LV setup, yielding peak-to-peak amplifier output voltage between $1.2\,\mathrm{V}$ and $7.4\,\mathrm{V}$. Such results confirm that the EMI filter components experience similar stress in the two cases, suggesting that the proposed setup is a viable solution for LV testing of VSCC AEFs for HV applications. Although the proposed test setup is not suitable for a complete EMI test, since the LV and HV sources are only equivalent at low-frequency, it provides a simple setup for AEF verification and tuning during pre compliance tests.

V. Conclusions

This paper presented a low-voltage test setup for the validation of Active EMI Filters intended for high-voltage applications. The proposed approach allows one to achieve operating conditions similar to those encountered in HV operation, while significantly reducing experimental complexity and safety constraints. Simulations and measurements were carried out on a VSCC Active EMI Filter test case. In both cases, the output voltage swing of the AEF power amplifier was found to be consistent between the proposed low-voltage setup and the corresponding high-voltage operating conditions. This agreement confirms that the proposed approach enables reliable evaluation of AEFs behavior using a low-risk test setup. The approach can therefore be effectively employed as a pre-validation stage prior to full-scale HV testing.

References

[1] J. Reimers, L. Dorn-Gomba, C. Mak, and A. Emadi, “Automotive Traction Inverters: Current Status and Future Trends,” *IEEE Transactions on Vehicular Technology*, vol. 68, no. 4, pp. 3337–3350, Apr. 2019.

[2] D. Han, S. Li, Y. Wu, W. Choi, and B. Sarlioglu, “Comparative Analysis on Conducted CM EMI Emission of Motor Drives: WBG Versus Si Devices,” *IEEE Transactions on Industrial Electronics*, vol. 64, no. 10, pp. 8353–8363, Oct. 2017.

[3] “CISPR 25:2021 - Vehicles, boats and internal combustion engines - Radio disturbance characteristics - Limits and methods of measurement for the protection of on-board receivers,” Dec. 2021.

[4] M. Fishta, E. Raviola, and F. Fiori, “EMI Reduction at the Source in WBG Inverters: A Comparative Study of Spread-Spectrum Modulation and Auxiliary Switching Leg Techniques,” *IEEE Transactions on Electromagnetic Compatibility*, pp. 1–8, 2024.

[5] B. Narayanasamy and F. Luo, “A Survey of Active EMI Filters for Conducted EMI Noise Reduction in Power Electronic Converters,” *IEEE Transactions on Electromagnetic Compatibility*, vol. 61, no. 6, pp. 2040–2049, Dec. 2019.

[6] M. L. Heldwein, H. Ertl, J. Biela, and J. W. Kolar, “Implementation of a Transformerless Common-Mode Active Filter for Offline Converter Systems,” *IEEE Transactions on Industrial Electronics*, vol. 57, no. 5, pp. 1772–1786, May 2010.

[7] S. Takahashi, “Simulation-Based Design of the Common-Mode Transformer-Less Hybrid EMI Filter in DC-Fed Motor Drive Systems,” *IEEE Access*, vol. 11, pp. 134 485–134 494, 2023.

[8] M. Fishta, P. Montorsi, and F. Fiori, “A Critical Analysis of Amplifier Requirements in Capacitance-Boosting Circuits for EMI Reduction,” in *2024 14th International Workshop on the Electromagnetic Compatibility of Integrated Circuits (EMC Compo)*, Oct. 2024, pp. 1–5.

[9] M. Fishta and F. Fiori, “A Volume-Optimized Hybrid EMI Filter for Automotive Traction Inverters,” *IEEE Transactions on Electromagnetic Compatibility*, vol. 68, no. 2, pp. 321–329, 2026.

[10] K. Kostov, “Design and characterization of single-phase power filters,” Ph.D. dissertation, Helsinki University of Technology, 2009.